DEM Corrections Before Unwrapping in a Small Baseline Strategy for InSAR Time Series Analysis

Gabriel Ducret, Marie-Pierre Doin, Raphaël Grandin, Cécile Lasserre, and Stéphane Guillaso

***Abstract*—Synthetic aperture radar interferometry (InSAR) is limited by temporal decorrelation and topographic errors, which can result in unwrapping errors in partially incoherent and mountainous areas. In this paper, we present an algorithm to estimate and remove local digital elevation model (DEM) errors from a series of wrapped interferograms. The method is designed to be included in a small baseline subset (SBAS) approach for InSAR time series analysis of ground deformation in natural environment. It is easy to implement and can be applied to all pixels of a radar scene. The algorithm is applied to a series of wrapped interferograms computed from ENVISAT radar images acquired across the Himalayan mountain range. The DEM error correction performance is quantified by the reduction of the local phase dispersion and of the number of residues computed during the unwrapping procedure. It thus improves the automation of the spatial unwrapping step.**

***Index Terms*—Digital elevation model (DEM) errors, interferometric synthetic aperture radar (InSAR), small baseline subset (SBAS).**

I. Introduction

THE Interferometric Synthetic Aperture Radar (InSAR) method has broadly fulfilled a long-standing need of the geophysical hazard research, which is to achieve a precise measurement of small ground displacements both at short and large spatial wavelengths [1]. However, single-pair InSAR suffers from atmospheric perturbations, topographic errors, and phase noise. Multi-temporal InSAR techniques have been developed to overcome some of these issues, taking profit from large time series of SAR data [2].

The permanent scatterers (PS) method detects individual scatterers carrying a reliable phase information over the whole SAR data stack [3]. However, in natural settings, the density of PS is generally insufficient. The small baseline subset (SBAS) strategy [4]–[6] exploits distributed scatterers (DS) by filtering out the non overlapping parts of the radar spectrum before interferogram formation with small perpendicular baselines. Further interferogram filtering and/or multi-looking limits the impact of temporal decorrelation. The SBAS method has been successfully applied in various natural settings [7], [8]. The SqueeSAR [9] and StaMPS-MTI methods [10] combine DS and PS in order to improve the spatial coverage of selected points. The latter is further increased by selecting only partially coherent scatterers [2], [9].

In these methods exploiting a large pile of coregistered differential interferograms, DEM errors can be systematically corrected based on the fact that they produce phase changes increasing linearly with the relative perpendicular baseline between acquisitions. In standard applications of the SBAS technique, once interferograms have been unwrapped, DEM corrections are estimated by inversion of a linear set of equations [11], [12]. The performance therefore relies on the success of a prior unwrapping step. However, DEM error contributions in differential interferograms can result both in phase discontinuities [13] and in apparent coherence loss when the perpendicular baseline is above 100–200 m, especially in mountainous areas. Therefore, correcting for DEM errors after phase unwrapping in SBAS approaches is not an optimal strategy.

In PS techniques, the DEM error, together with the ground velocity, is estimated directly on the differential wrapped phase information between neighboring pixels organized in a sparse network [3]. Similarly, in [14], the local DEM error estimation is embedded in the minimum cost flow unwrapping algorithm, extended in the time domain to include the small baseline interferometric network. Here, as in [10], we propose to extract local DEM errors from wrapped interferograms with varying perpendicular baselines. However, we do not select a sparse network of a priori stable points. We rather show the feasability of computing complete maps of local DEM errors and temporal coherence. The phase information contained in moderately or partially coherent pixels can then easily be exploited by further spatial filtering (possibly based on temporal coherence), aided by the phase scatter reduction due to DEM correction [15]. The purpose is to improve the spatial unwrapping step of interferograms processed with an SBAS strategy.

In Section II, we present the DEM correction algorithm and point out similarities and differences with respect to previously published work. It is applied in Section III to a series of coregistered, wrapped interferograms. We then quantify how the DEM correction reduces the local phase variability and improves the later unwrapping step.

Manuscript received July 5, 2012; revised January 4, 2013 and May 3, 2013; accepted July 3, 2013. This work was supported by the Institut National des Sciences de l'Univers (PNTS) and Agence Nationale de la Recherche (ANR) via project EFIDIR (ANR-07-MDC0-004).

G. Ducret is with Laboratoire de Géologie, Ecole Normale Supérieure, 75231 Paris, France (e-mail: ducret@geologie.ens.fr).

M.-P. Doin and C. Lasserre are with the Institut des Sciences de la Terre (ISTerre), Université de Grenoble 1, CNRS 38041 Grenoble, France (e-mail: marie-pierre.doin@ujf-grenoble.fr; cecile.lasserre@ujf-grenoble.fr).

R. Grandin is with Institut de Physique du Globe de Paris, Sorbonne Paris Cité, Univ Paris Diderot, UMR 7154 CNRS, F-75005 Paris, France (e-mail: grandin@ipgp.fr).

S. Guillaso is with the Computer Vision and Remote Sensing, Technische Universität Berlin, 10587 Berlin, Germany (e-mail: stephane.guillasotu-berlin.de).

Color versions of one or more of the figures in this paper are available online at http://ieeexplore.ieee.org.

Digital Object Identifier 10.1109/LGRS.2013.2276040

II. DEM Correction Algorithm

A. General Setting

Let us consider differential interferograms formed by two images acquired at dates k and l, with perpendicular baselines $B_\perp^{kl}$. ϕ refers to the wrapped differential interferometric phase, whereas φ refers to the unwrapped phase. In the following, the superscripts kl on ϕ or $B_\perp$ refer to the kth and lth images forming an interferogram, whereas a single superscript k denotes φ or $B_\perp$ of the kth image. We assume that the flat earth and topographic contributions have been removed from the interferometric phase, using precise orbits and a DEM. The differential interferometric phase ϕ^{kl} still includes various contributions

$$\phi^{kl} = \phi^{kl}_{displ} + \phi^{kl}_{atm} + \phi^{kl}_{res,orb} + \phi^{kl}_{res,topo} + \phi^{kl}_{noise} \quad (1)$$

where ϕ^{kl}_{displ} is the ground displacement contribution in the radar line of sight (LOS), ϕ^{kl}_{atm} is the atmospheric delay, $\phi^{kl}_{res,orb}$ is the residual flat earth contribution, $\phi^{kl}_{res,topo}$ is the residual topographic contribution, and ϕ^{kl}_{noise} is the phase noise due to temporal decorrelation or changes in the radar look angle. The residual topographic term, $\phi^{kl}_{res,topo}$, depends on the DEM height error, δh_{err}

$$\phi^{kl}_{res,topo} \equiv \frac{4\pi}{\lambda}\frac{B^{kl}_\perp}{R\sin\theta}\delta h_{err}[2\pi] \quad (2)$$

where λ is the radar wavelength (5.6 cm for ENVISAT C-band acquisition), θ is the local incidence angle, and R is the range. Note that proportionality between ϕ and $B_\perp$ in the above equation is known modulo 2π, hence producing a nonlinear problem.

B. Algorithm

As in [3], [16], we assume that the residual orbital contribution, the atmospheric delay, and the deformation are spatially correlated at a local scale. The differential phase series, $\delta\phi^{kl}$, w.r.t. a nearby reference, is thus approximated by

$$\delta\phi^{kl} \approx \left(\delta\alpha B^{kl}_\perp + \beta\right)[2\pi] \quad (3)$$

where β is a phase offset and where the relative DEM error coefficient, $\delta\alpha$, is defined by

$$\delta\tilde{\alpha} = \frac{4\pi}{\lambda R\sin\theta}(\delta h_{err} - \delta h_{ref}). \quad (4)$$

The phase offset, β, should tend to the average deformation included in employed interferograms relative to the reference pixel. The phase scatter in (3) that results from neglecting deformation is reduced if the average temporal baseline, Δt, of included interferograms is small: differential LOS velocity should not exceed $\lambda/(8\Delta t)$. In case of larger local deformation gradients, a deformation term should be added to the phase analysis. Biased estimates of α and partial removal of the deformation may occur in the unlikely case where the local deformation signal in included interferograms is correlated with their perpendicular baselines.

In PS approaches, double difference phase series are defined between neighboring PS organized in a sparse network (for example by Delaunay triangulation) [3]. In StamPS, high-pass filtering of the phase of PS candidates provides the necessary local referencement for phase time series [10]. Alternatively, we here divide the interferograms in overlapping subwindows (typically, 1000 to 2000 m wide in C-band) and select as a reference the pixel that presents, on each subwindow, the highest spatial coherence, γ_s, averaged on the series of computed SBAS interferograms.

In each subwindow, and for each pixel, we then compute $\delta\alpha$ in three steps:

1) A first estimate of $\delta\tilde{\alpha}$, $\delta\tilde{\alpha}_{raw}$, is obtained by a discrete search of $\delta\tilde{\alpha}$ in an imposed interval [14], [16], where one maximizes the temporal coherence, γ_t:

$$\gamma_t e^{i\beta} = \left(\sum w^{kl} e^{i\delta\phi^{kl}}\left(e^{i\delta\alpha B^{kl}_\perp}\right)^*\right)/\sum w^{kl}. \quad (5)$$

The weight, w^{kl}, taken as $e^{-B^{kl}_t/N_{days}}$, depends on the temporal baseline B_t expressed in days, where N_{days} corresponds approximately to the decorrelation time.

2) A refined estimate of $\delta\tilde{\alpha}$, $\delta\alpha_{ls}$, is computed from the phase residues: $e^{i\delta\phi^{kl}_{res}} = e^{i(\delta\phi^{kl} - \delta\alpha_{raw}B^{kl}_\perp - \beta)}$, assuming that the residues, $\delta\phi^{kl}_{res}$, are included in the $[-\pi,\pi]$ interval. The equation $\delta\phi^{kl}_{res} = \delta\alpha_{res}B^{kl}_\perp + \beta_{res}$ is now linear and is inverted by least mean square. We then obtain

$$\delta\alpha_{ls} = \delta\alpha_{raw} + \delta\alpha_{res}. \quad (6)$$

3) Finally, a temporal inversion on the new phase residues, $\delta\phi^{kl}_{res}$, again assumed to be in the $[-\pi,\pi]$ interval, allows to compute a series of unwrapped differential phase $\delta\varphi^k_{res}$, one per acquisition k. Because we select interferograms that cover the whole perpendicular baseline spread but are possibly limited in temporal baseline, we add constraints to the inverted system [7]

$$W\begin{bmatrix} -1 & 1 & 0 & 0 & 0 & 0 \\ -1 & 0 & 0 & 1 & \vdots & \vdots \\ \vdots & \vdots & \vdots & \vdots & \vdots & \vdots \\ 0 & 0 & -1 & 1 & 0 & 0 \\ 1 & \dots & \dots & 1 & 0 & 0 \\ 1 & & & 0 & -B^1_\perp & -1 \\ & \ddots & & & \vdots & \vdots \\ & & \ddots & & \vdots & \vdots \\ 0 & & & 1 & -B^n_\perp & -1 \end{bmatrix}\begin{bmatrix} \delta\varphi^1_{res} \\ \vdots \\ \vdots \\ \delta\varphi^n_{res} \\ \delta\alpha'_{res} \\ \beta'_{res} \end{bmatrix} = W\begin{bmatrix} \delta\phi^{kl}_{res} \\ \vdots \\ \vdots \\ \vdots \\ 0 \\ \vdots \\ \vdots \\ \vdots \\ 0 \end{bmatrix} \quad (7)$$

where the vector, W, weights the first M interferogram data lines by w_{kl} and the following N constraint lines by 0.01. Additional constraints, however, with a small weight, allow avoiding rank deficiencies and fixing the unknown phase shifts between independent groups of images to the values that provide the best linear relationship between phase and perpendicular baseline. At this stage, we obtain a corrected DEM error coefficient, $\delta\alpha_f = \delta\alpha_{ls} + \delta\alpha'_{res}$, relative to the reference pixel of each subwindow.

The relative DEM error coefficients obtained in sliding subwindows, $\delta\alpha_f$, must then be mosaicked. To avoid integration that could propagate errors across areas of low coherence, we

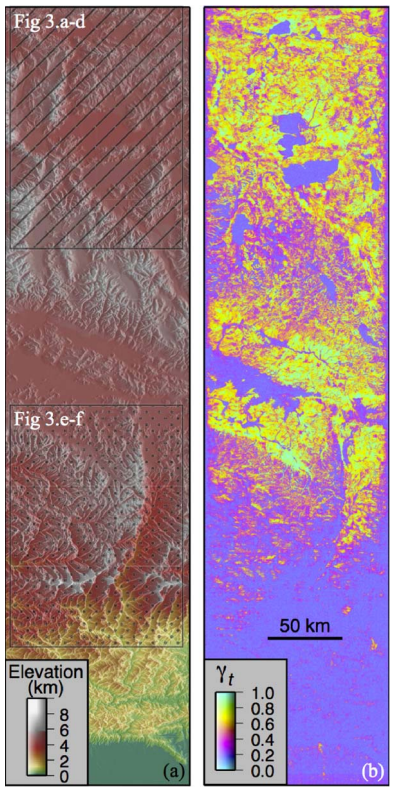

Fig. 1. (a) SRTM relief map of the study area. (b) Temporal coherence.

simply take the median value of the DEM errors within each subwindow, weighted by the pixel temporal coherence, and substract it from all DEM errors of this window. This high-pass median filter applied to DEM errors can be seen as an equivalent to the spatially uncorrelated DEM error of [10]. The residual low-pass DEM error component will later be more easily retrieved once interferograms are unwrapped and analyzed in time series. Damping is then applied across the overlapping parts of the sliding windows to adjust the DEM corrections over the whole SAR image. Finally, we apply to the DEM error map a low-pass filter and a mask adapted to the temporal coherence to remove DEM error outliers in incoherent areas. For $\gamma_t > 0.35$, no filtering is applied. Below a threshold of 0.2, the DEM error is replaced by the result of an averaging kernel of Gaussian shape weighted by temporal coherence. In the interval [0.2, 0.35], the applied filter decreases linearly between the described Gaussian filtering and no filtering.

III. Application and Validation

A. Data and Interferogram Processing

The algorithm is tested on a descending ENVISAT track (track 119), which covers from North (32° N) to South (27° N) the Southern part of the Tibetan Plateau, the Himalayan range, and the northernmost Indo-Gangetic plain [Fig. 1(a)] at a longitude of 84° E. This variably vegetated area has an extremely rough relief across the Himalaya but is only moderately mountainous to the North. The ENVISAT archive consists of 29 Envisat SAR images acquired from 2003 to 2010 with a total perpendicular baseline spread of 1500 m (Fig. 2).

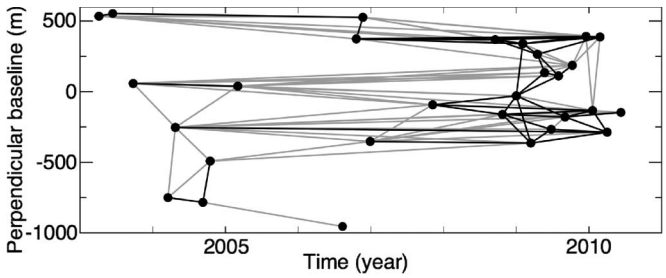

Fig. 2. Interferometric network. Each line linking SAR images represents a computed interferogram while the dark lines show the interferograms selected to process DEM corrections.

Differential interferograms are generated using a SBAS processing chain [17] based on the Repeat Orbit Interferometry PACkage (ROI_PAC) software [18] with the following characteristics:

1) Based on precise DORIS orbits and the DEM in radar geometry, we compute a priori range distortion maps between master and slave images. All Single Look Complex (SLCs) are coregistered to a common master radar geometry using these a priori range distortion maps and regularized offset fields in azimuth derived from amplitude image correlation. This precise coregistration of all SLCs is a crucial prerequisite to allow for correction of DEM errors on a pixelwise basis.
2) The series of SLCs in a common master geometry is used to compute a series of SBAS differential interferograms (Fig. 2). The SLCs range spectrum is restricted to the overlapping spectrum for the two acquisitions, with a slope adaptative algorithm [19], [20].
3) Because of the strong decorrelation across the Himalayan range and to the South [Fig. 1(b)], we multi-look the small baseline interferograms by a factor 4x20 before DEM error computation. However, multi-looking before DEM correction degrades the expected gain of DEM correction in terms of phase scatter reduction, useful for later processing steps (filtering and unwrapping). Therefore, in more favorable environments, multi-looking should be applied only after DEM correction.
4) One must then select the interferograms presenting the least temporal decorrelation, the correction being applied subsequently to all interferograms. Surprisingly, the coherence across the Himalayas may be preserved in some cases for up to 3 years, depending on the seasonal and interannual monsoon fluctuations. We thus select the 36 most coherent interferograms out of 99 interferograms, independently of their temporal baseline [Fig. 2].
5) Finally, the stratified atmospheric contribution predicted from the ERA-Interim European Centre for Medium-Range Weather Forecasts (ECMWF) reanalysis [21], [22] and a phase ramp are removed from the interferograms.

B. DEM Correction

We present in Fig. 3 a zoom of the northern part of the track, showing the DEM error map, the temporal coherence map, and one example of an interferogram at 35 days and

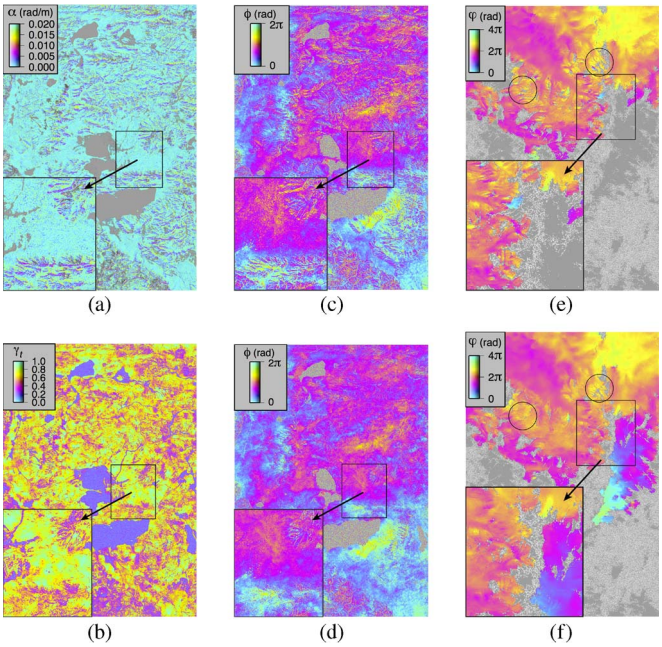

Fig. 3. (a) Map of the DEM error coefficient (in rad/m). (b) Map of the temporal coherence. (c) Original differential interferogram with a perpendicular baseline of 300 m and a temporal baseline of 35 days (d). Interferogram after DEM error correction. (a–d) Zoom location shown on Fig. 1. (e), (f) Comparison of the unwrapped phase before (e) and after (f) DEM correction (Zoom location shown on Fig. 1). The cuts are overlaid in white on the unwrapped interferograms and on the gray areas that have not been reached by the unwrapping algorithm.

with a large perpendicular baseline (around 300 m). Orographic structures are easily recognized in the DEM error map. The correction is set to zero in areas with very low coherence and is highest in mountainous areas, especially along crests and gullies slopes. The temporal coherence map highlights the contours of lakes, marshes, and rivers. Thin linear structures with either high or low coherence are efficiently extracted. The comparison between the original and corrected differential interferogram [Fig. 3(c) and (d)] shows that most of the residual topographic features are successfully corrected except in areas of low temporal coherence where the retrieved correction is not reliable.

C. Local Phase Variability

In order to quantify the efficiency of the DEM error correction to reduce the local phase variability, we systematically analyze the phase standard deviation, σ_ϕ, in small square subwindows of all interferograms before and after correction. The subwindows must be large enough to include the topographic structures that have been corrected, but must be smaller than the scale of unmodeled processes, such as turbulent atmospheric patterns, deformation, or orbital errors. Here, we compute in 20×20 subwindows the ratio of the local phase standard deviation before and after correction, together with the average value of the temporal coherence. An average of these ratios over the whole interferogram is then plotted as a function of increasing average temporal coherence [blue dots in Fig. 4(a)]. Not surprisingly, the reduction of the local phase variability increases with the temporal coherence. Improvement of

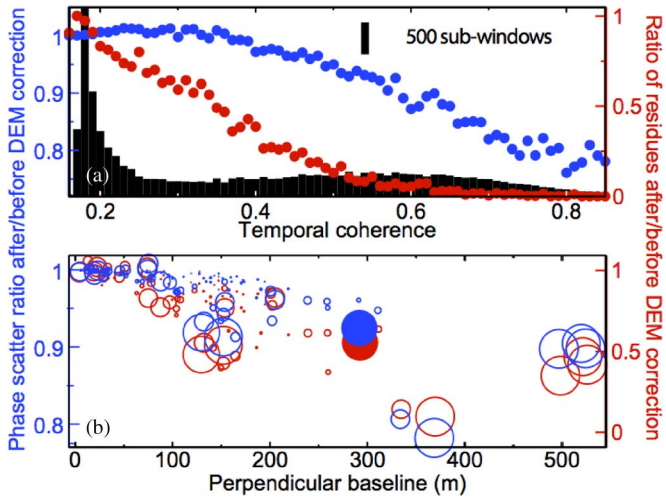

Fig. 4. Effect of DEM correction on phase scatter and on the number of residues. (a) The reduction of local phase scatter (blue) and of the number of residues (red) before and after DEM error correction is displayed as a function of the temporal coherence averaged in subwindows, for the interferogram shown on Fig. 3. The histogram of temporal coherence averaged in 20×20 windows is shown in black. (b) Average phase scatter reduction (in blue) and average ratio of the number of residues (in red) as a function of perpendicular baseline. Each circle represents an interferogram, and its size is inversely proportional to the temporal baseline. The filled circles correspond to the example shown in panel (a).

the interferometric phase scatter is thus limited by temporal decorrelation that destroys the phase informative content. The average phase scatter reduction, selecting subwindows with a coherence larger than 0.3, is also shown for each interferogram as a function of the perpendicular baseline in Fig. 4(b). No improvement occurs for perpendicular baselines below 50 m, whereas for $B_\perp$ between 50 and 500 m, the phase scatter reduction increases with the perpendicular baseline, reaching 10–25% for the largest perpendicular baselines. Note that interferograms with $B_\perp$ larger than 400 m are strongly affected by geometrical decorrelation in this area of large relief.

D. Unwrapping

In order to quantify how the correction improves phase unwrapping, we apply the same unwrapping cut-tree algorithm [23] to all interferograms with and without the DEM error correction. The number of residues can be used as a statistical proxy for the unwrapped surface and probability of occurrence of an unwrapping error. The ratio of the number of residues after/before DEM correction is computed in small square subwindows and plotted as a function of the subwindow temporal coherence [red dots in Fig. 4(a)]. The residues reduction strongly increases with coherence. This effect is explained by the phase scatter reduction at small wavelength. We also plot in Fig. 4(b) the average ratio of the number of residues before and after DEM correction as a function of perpendicular baseline, excluding areas with very low coherence ($\gamma_t < 0.3$). The ratio decreases from 0.9 to 0.4 for perpendicular baseline from 0 to 150 m, and is below 0.5 for $B_\perp > 300$ m. The number of cuts is thus significantly reduced in the corrected interferograms, yielding a larger unwrapped surface and a lower probability for unwrapping errors [see Fig. 3(e) and (f)].

IV. Conclusion

In this paper, we present an algorithm to correct DEM errors in a series of wrapped interferograms and to estimate a temporal coherence map. It differs from previously published methods mainly because it is designed for being easily applied to all pixels of a radar scene without a priori pixel selection, thus preserving the complete spatial content of corrected interferograms. It is thus meant to be included in standard "SBAS" InSAR processing chains, where phase reliability before unwrapping is increased by spatial filtering and/or multi-looking (by contrast to a pixel selection strategy).

The algorithm is tested in this paper on Envisat interferograms crossing the Himalayan range. We show that the DEM correction allows to significantly reduce the local phase variability and the number of phase residues for large baseline interferograms. It facilitates spatial unwrapping, leading to larger unwrapped surfaces and less unwrapping errors. As this step still requires visual checking and manual intervention, any improvement in the unwrapping automation should speed up the overall processing of multi-temporal InSAR data.

Acknowledgment

R. Grandin post-doc fellowship was provided by CNES. Data were obtained through the ESA-MOST Dragon project (id 5305).

References

[1] R. Bürgmann, P. A. Rosen, and E. J. Fielding, "Synthetic aperture radar interferometry to measure Earth's surface topography and its deformation," *Annu. Rev. Earth Planet. Sci.*, vol. 28, no. 1, pp. 169–209, May 2000.

[2] A. Hooper, D. Bekaert, K. Spaans, and M. Arkan, "Recent advances in SAR interferometry time series analysis for measuring crustal deformation," *Tectonophysics*, vol. 514/517, pp. 1–13, Jan. 2012.

[3] A. Ferretti, C. Prati, and F. Rocca, "Permanent scatterers in SAR interferometry," *IEEE Trans. Geosci. Remote Sens.*, vol. 39, no. 1, pp. 8–20, Jan. 2001.

[4] P. Berardino, G. Fornaro, R. Lanari, and E. Sansosti, "A new algorithm for surface deformation monitoring based on small baseline differential SAR interferograms," *IEEE Trans. Geosci. Remote Sens.*, vol. 40, no. 11, pp. 2375–2383, Nov. 2002.

[5] S. Usai, "A least squares database approach for SAR interferometric data," *IEEE Trans. Geosci. Remote Sens.*, vol. 41, no. 4, pp. 753–760, Apr. 2003.

[6] D. A. Schmidt and R. Bürgmann, "Time-dependent land uplift and subsidence in the Santa Clara valley, California from a large interferometric synthetic aperture radar data set," *J. Geophys. Res., Solid Earth*, vol. 108, no. B9, pp. 2416–2429, Sep. 2003.

[7] P. López-Quiroz, M.-P. Doin, F. Tupin, P. Briole, and J.-M. Nicolas, "Time series analysis of Mexico City subsidence constrained by radar interferometry," *J. Appl. Geophys.*, vol. 69, no. 1, pp. 1–15, Sep. 2009.

[8] R. Lanari, F. Casu, M. Manzo, G. Zeni, P. Berardino, M. Manunta, and A. Pepe, "An overview of the small BAseline subset algorithm: A DInSAR technique for surface deformation analysis," *Pure Appl. Geophys.*, vol. 164, no. 4, pp. 637–661, Apr. 2007.

[9] A. Ferretti, A. Fumagalli, F. Novali, C. Prati, F. Rocca, and A. Rucci, "A new algorithm for processing interferometric data-stacks: SqueeSAR," *IEEE Trans. Geosci. Remote Sens.*, vol. 49, no. 9, pp. 3460–3470, Sep. 2011.

[10] A. Hooper, "A multi-temporal InSAR method incorporating both persistent scatterer and small baseline approaches," *Geophys. Res. Lett.*, vol. 35, no. 16, pp. L16302-1–L16302-5, Aug. 2008.

[11] S. Samsonov, "Topographic correction for ALOS PALSAR interferometry," *IEEE Trans. Geosci. Remote Sens.*, vol. 48, no. 7, pp. 3020–3027, Jul. 2010.

[12] A. Pepe, B. Ortiz, P. Lundgren, P. A. Rosen, and R. Lanari, "The Stripmap-ScanSAR SBAS approach to fill gaps in stripmap deformation time-series with ScanSAR data," *IEEE Trans. Geosci. Remote Sens.*, vol. 49, no. 12, pp. 4788–4804, Dec. 2011.

[13] H. A. Zebker and J. Villasensor, "Decorrelation in interferometric radar echoes," *IEEE Trans. Geosci. Remote Sens.*, vol. 30, no. 5, pp. 950–959, Sep. 1992.

[14] A. Pepe and R. Lanari, "On the extension of the minimum cost flow algorithm for phase unwrapping of multitemporal differential SAR interferograms," *IEEE Trans. Geosci. Remote Sens.*, vol. 44, no. 9, pp. 2374–2383, Sep. 2006.

[15] R. Grandin, M. Doin, L. Bollinger, B. Pinel-Puyssegur, G. Ducret, R. Jolivet, and S. Sapkota, "Long-term growth of the Himalaya inferred from interseismic InSAR measurement," *Geology*, vol. 40, no. 12, pp. 1059–1062, Dec. 2012.

[16] A. Hooper, H. Zebker, P. Segall, and B. Kampes, "A new method for measuring deformation on volcanoes and other natural terrains using InSAR persistent scatterers," *Geophys. Res. Lett.*, vol. 31, no. 23, pp. L23611-1–L23611-5, Dec. 2004.

[17] M. P. Doin, S. Guillaso, R. Jolivet, C. Lasserre, F. Lodge, G. Ducret, and R. Grandin, "Presentation of the small baseline NSBAS processing chain on a case example: The Etna deformation monitoring from 2003 to 2010 using Envisat data," in *Proc. Fringe Meet.*, 2011, pp. 1–7.

[18] P. A. Rosen, S. Henley, G. Peltzer, and M. Simons, "Update repeat orbit interferometry package released," *EOS Trans.*, vol. 85, no. 5, pp. 47–47, Feb. 2004.

[19] F. Gatelli, A. M. Guarnieri, F. Parizzi, P. Pasquali, C. Prati, and F. Rocca, "Wavenumber shift in SAR interferometry," *IEEE Trans. Geosci. Remote Sens.*, vol. 32, no. 4, pp. 855–865, Jul. 1994.

[20] G. Davidson and R. Bamler, "Multiresolution phase unwrapping for SAR interferometry," *IEEE Trans. Geosci. Remote Sens.*, vol. 37, no. 1, pp. 163–174, Jan. 1999.

[21] M.-P. Doin, C. Lasserre, G. Peltzer, O. Cavalié, and C. Doubre, "Corrections of stratified tropospheric delays in SAR interferometry: Validation with global atmospheric models," *J. Appl. Geophys.*, vol. 69, no. 1, pp. 35–50, Sep. 2009.

[22] R. Jolivet, R. Grandin, C. Lasserre, M.-P. Doin, and G. Peltzer, "Systematic InSAR tropospheric phase delay corrections from global meteorological reanalysis data," *Geophys. Res. Lett.*, vol. 38, no. 17, pp. L17311-1–L17311-6, Sep. 2011.

[23] R. M. Goldstein, H. A. Zebker, and C. Werner, "Satellite radar interferometry: Two-dimensional phase unwrapping," *Radio Sci.*, vol. 23, no. 4, pp. 713–720, Jul./Aug. 1988.